

# A Multiresolution Deep Learning Framework for Automated Annotation of Reflectance Confocal Microscopy Images

Kivanc Kose\*, Alican Bozkurt \*\*, Christi Alessi-Fox \*\*\*, Melissa Gill\*\*\*\*,  
Dana H. Brooks \*\*, Jennifer G. Dy \*\*, Milind Rajadhyaksha\*

\*Dermatology Service, Memorial Sloan Kettering Cancer Center, New York, NY, USA, \*\*Electrical and Computer Engineering Department, Northeastern University, Boston Massachusetts, \*\*\*CaliberID, Rochester, NY, USA, \*\*\*\*Skin Medical Research and Diagnostics P.L.L.C., Dobbs Ferry, NY, USA  
[kosek@mskcc.org](mailto:kosek@mskcc.org)

**Abstract:** Morphological tissue patterns in RCM images are critical in diagnosis of melanocytic lesions. We present a multiresolution deep learning framework that can automatically annotate RCM images for these diagnostic patterns with high sensitivity and specificity.

**OCIS codes:** (100.4996) Pattern recognition, neural networks, (170.1790) Confocal microscopy (170.1870) Dermatology (150.1135) Algorithms

## 1. Introduction

Approximately 3.6 million new cases of skin cancer are diagnosed in the USA every year, and another million worldwide [11]. The current gold standard in diagnosis is biopsy followed histology, which is an invasive, costly and laborious procedure. Moreover, biopsy-based workflow is inefficient: the benign-to-malignant biopsy ratios still range from as low as 2-to-1 to as high as 600-to-1 depending on the clinical setting and the experience level of the clinician, even after “preselection” using clinical imaging and dermoscopy [2]. Recent advances in in-vivo microscopy offer non-invasive, cost-effective and efficient ways of examining tissue morphology and cytology. Among several available methods, reflectance confocal microscopy (RCM) stands out offering resolution and sectioning comparable to histology. Diagnostic information in RCM images, similar to histology, is based on the morphological and cytological appearance of the tissue under the microscope. Whereas histology images contain color contrast due to the staining agents, RCM images are grayscale with the difference between reflective properties of the tissue components being the source of contrast. Lack of tissue-specific color contrast makes RCM images harder to analyze compared to histology. Even though users, who were involved in the early clinical development of RCM, can read these with high sensitivity and specificity, the newer cohort of -novice- users struggles to achieve the same level of confidence in their analysis. They typically need extensive training and guidance in order to reach the level of the early adopters.

Unlike traditional black box approaches that are capable of classifying a lesion as malignant vs. benign, here we offer a framework that can segment different morphological patterns that are encountered in RCM images collected at dermal epidermal junction (DEJ) level of melanocytic lesions. In this way, rather than giving a blind diagnostic support to the clinicians, we aim to help them to learn these morphological patterns and become more confident about their diagnostic decisions. The proposed framework works as a diagnostic support system, by highlighting potential suspicious regions for further examination. In this way, we aim to make RCM based clinical practice more efficient by limiting the tissue regions to be analyzed.

## 2. Methods

We propose a new hierarchical encoder-decoder based semantic segmentation network structure that is composed of multiple U-Net subnetworks in a cascaded fashion. With the proposed network architecture, we aim to solve the segmentation problem at different resolutions and merge the results (from coarse-to-fine) in order to obtain the final high-resolution segmentation. Similar models in the literature use independent networks trained over different resolution versions of the data, ensemble over the results of individual networks to obtain the final segmentation. The novelties of the proposed architecture are (i) we cascade the individual U-Nets in such a way that coarser-level segmentations are utilized by the following finer-level segmentation networks together with the data (see Fig. 1) and (ii) we calculate and backpropagate the loss at the intermediate levels to increase the efficiency and speed of training the early levels of the model.

Proposed network is composed of 3 U-Net [3] subnetworks cascaded in a hierarchical manner. However, it can be generalized to contain more or fewer levels depending on the needs and computational capabilities. Our 3-level model is illustrated in Figure 1(left). The input to the first level ( $Unet_4$ ) of the network is the 4-times down-sampled version ( $L_4$ ) of the original image ( $I_0$ ). We used a modified U-Net structure (Figure 1, right) to predict the respective segmentation. The output of  $Unet_4$  is compared against 4 times downsampled version of the label map and first level loss ( $Loss_4$ ) is calculated. At the end of this stage, we introduce our first novelty; concatenating the upsampled version of the Level-1 segmentation result ( $L_4$ ) with 2-times down-sampled version of the data ( $I_2$ ) and feeding them together into second level ( $Unet_2$ ) of the network.

By feeding the coarser level segmentation output to the next level, we actually introduce a prior subnetwork segmentation (except level-1) and allow the overall model to improve the results of the coarser estimations. Moreover, we observe that such topology helps in obtaining more coherent segmentation, which avoids over-segmentation, and formation of very small, isolated label clusters. Here, we repeat this process 2 times and obtain a 3-level topology. In order to increase the detail level

of the segmentation, we increase the depth of the UNet subnetworks at each level by one. The resulting 3-level network is composed of ~50 layers and ~6M learnable parameters.

Training such deep networks is known to be problematic due to vanishing gradients. As the error is backpropagated in deeper networks, the gradient diminishes and the updates on the network parameters become very small, resulting in slow training. In order to overcome this issue, we calculate and backpropagate the error between intermediate segmentation results and the down-sampled version of the ground truth segmentation (we call this “error injection”). In this way, we (i) obtain better access to the gradients of the deeper portions of the network as well as, (ii) we control the behavior of the network at the earlier stages and help it to obtain better priors for the later stages of the topology.

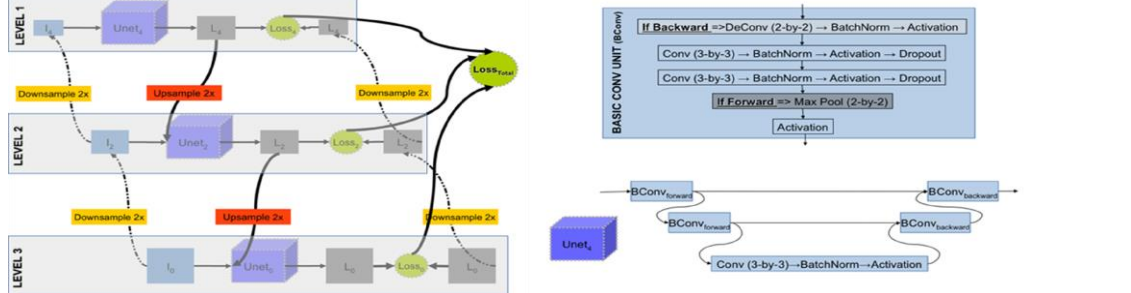


**Figure 1:** Our network topology (left) is composed of 3 cascaded UNet networks, that generate semantic segmentations at different resolutions. Low-resolution segmentations are used as priors for high-level segmentation networks. The U-Net topology used at level 1 and basic convolutional layer (BConv) are presented on the right side.

### 3. Results and Conclusions

Our dataset is composed of 70 RCM mosaics (covering 16-36mm<sup>2</sup> area), collected from “melanoma suspicious” lesions. The mosaics are consensus labeled by 2 expert readers for 6 different labels; *Non-Lesion, Artifact, Meshwork Pattern, Ring Pattern, Nested Pattern, and Patternless*. We divide the dataset into 2 distinct sets of training and testing. We randomly pick mosaics from the whole dataset and set mosaics (~30%) of the dataset for testing and the rest for training. Mosaics are too large in image size (16-to-24MP) to be processed as a whole, therefore, at every epoch, we extract random patches from the mosaics and input them to the segmentation network. We cover the whole mosaic area, by extracting 0.5-0.5 mm sized patches from every 1mm-by-1mm with 50% overlap in a sliding window fashion. In order to further improve the training efficiency, we also increase the training data amount using data augmentation (random rotation, flipping, shearing and mean intensity level change). We trained the described model using Keras framework.

In Figure 2, we present example segmentation results obtained using the trained model. Training of the network took almost a day on a 12GB NVIDIA TITANX graphics processing unit (GPU). On the other hand, testing is very fast. Using the same GPU configuration, it only takes around 30 secs for the whole mosaic to be pixelwise annotated.

Applying the model overall test set, we achieved [0.72, 0.77, 0.24, 0.77, 0.94, 0.90] sensitivity and [0.97, 0.97, 0.98, 0.97, 0.87, 0.91] specificity for each individual label respectively. The results show that the segmentation model performs quite well automatically annotation the diagnostic labels except the meshwork pattern. Further comparison of the model outputs with the ground truth labels show that the model confuses meshwork pattern with ring pattern and patternless classes. Visual examination of the results confirms that most of the wrongly classified meshwork pattern contains deformed variations of the pattern, which can also be misclassified by novice readers. We believe that it is possible to overcome this problem by using more training data of meshwork pattern that contains such deformations.

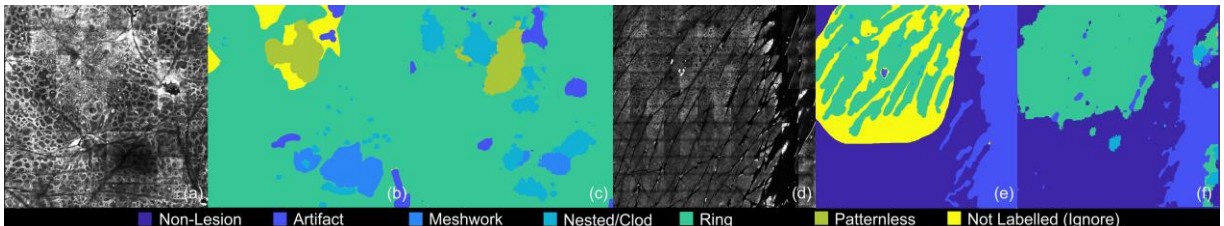


**Figure 2:** Example segmentation results of images (a) and (d). The ground truth segmentation of the expert reviewers (b) and (e) are side by side compared to the algorithmic results (c) and (f). Images are not exhaustively annotated by the expert readers. Pixels that are not annotated (yellow label) are ignored during training. During the testing phase, these are discarded from sensitivity and specificity calculations.

### 4. References

- [1] V. Nikolaou and A. J. Stratigos, “Emerging trends in the epidemiology of melanoma,” *The British journal of dermatology*, vol. 170, no. 1, pp. 11–19, Jan. 2014.
- [2] M. Rajadhyaksha, A. Marghoob, A. Rossi, A. C. Halpern, and K. S. Nehal, “Reflectance confocal microscopy of skin in vivo: From bench to bedside..,” *Lasers in surgery and medicine*, vol. 49, no. 1, pp. 7–19, Jan. 2017.
- [3] O. Ronneberger, P. Fischer, and T. Brox, “U-Net: Convolutional Networks for Biomedical Image Segmentation,” in *Medical Image Computing and Computer-Assisted Intervention – MICCAI 2015*, Springer International Publishing, 2015, pp. 234–241.